AN EXTREME ULTRAVIOLET PHOTOEMISSION STUDY

NSR 33-144-002

FINAL REPORT

Submitted by:

Dr. Robert M. Finn
Research Scientist

Materials Science Laboratory
SYRACUSE UNIVERSITY RESEARCH CORPORATION
Merrill Lane, University Heights
Syracuse, New York 13210

December 10, 1969

ABSTRACT

The photoemissive properties of Fe, Mo, Cu, Ni, and Al have been investigated at the wavelengths 584 Å, and 1216 Å. Radiation from a Hinterreger-type discharge lamp, employing He or H_2 as required, was dispersed in a 1-meter vacuum monochromator, and the appropriate wavelengths were made incident on samples which had undergone a wide range of plastic deformation. Both the photoelectric yield and the energy distribution of emitted electrons were correlated with the defect concentrations existing in these samples.

The yield of Al at 584 Å decreased monotonically, while that for Al at 1216 Å went through an obvious maximum before decreasing. The yield of Ni at 1216 Å varied unpredictably, though it tended toward lower values with increasing defect concentration. Other yields were approximately constant, though the observations cannot be considered final because of limitations in the experimental approach. These are discussed, and some general effects are described, as are the needed remedies.

The electron energy spectra were determined to be relatively independent of dislocation density except for the very obvious changes apparent in Mo at 1216 Å. The observed variations were too large to be attributed to instrumental uncertainties, and do represent real effects.

FOREWORD

The research described herein was performed by personnel of the Materials Science Laboratory of Syracuse University Research Corporation, under NASA Contract NSR 33-144-002, with Dr. Robert Fellows, Office of Planetary Atmospheres, NASA-Washington, D.C., as Project Monitor.

The program was initially proposed and conducted by Mr. Ken Damon, director of the Instrumentation Laboratory, beginning June 1968. Upon Mr. Damon's resignation from the Corporation in December 1968, the work was transferred to the Materials Science Laboratory and there continued by the laboratory director, Dr. Robert Aldrich. Dr. Robert Finn joined the laboratory in March 1969 and assumed principal responsibility for further experimental work, concluding in May of that year.

Dr. Volker Weiss of Syracuse University has participated continually in the program from the beginning, and his student, Mr. Ziya Bulun, has assisted in the preparation and characterization of all samples.

CONTENTS

LIST OF TABLES

LIST OF ILLUSTRATIONS

1 INTRODUCTION AND BACKGROUND

1.1 The Photoemissive Process

The mechanisms which govern photoemission stimulated by extreme ultraviolet (EUV) radiation are rather well understood in principle.[1-7] If the EUV radiation is incident with intensity I_o on a surface, the intensity I(x) at any depth x depends upon the intensity attenuation coefficient α and the surface reflectance ρ,

$$I(x) = (1-\rho)\ I_o \exp(-\alpha x).$$

Though it may vary widely, a typical figure for α is $\sim 10^6 cm^{-1}$. ρ likewise varies widely, being sensitive to surface topography, wavelength, and angle of incidence.

I(x) is also representative of the initial spatial distribution of photo-excited electrons if $d\alpha/dx = 0$. For firstorder treatment, it is generally assumed that the crystal momentum vectors of those electrons are distributed isotropically. It is further assumed that the inelastic scattering, which degrades the electron energy, is also isotropic. The rationale of these and other assumption has been treated in the literature by Berglund and Spicer[6] and Kane[7] among others.

Clearly, it is not sufficient for emission that an electron within the EUV target be stimulated to an energy level exceeding the vacuum level of that material. The electron must also 1) possess a crystal momentum component p_z normal to the emitting surface such that $p_z^2/2m + V \geq 0$, where V is the local (averaged) potential; 2) experience no elastic or inelastic collisions which result in $p_z < \sqrt{-2mV}$ in its path to the surface; 3) successfully transit the surface potential barrier at which there exists a finite probability R of reflection.

These factors have been treated[6-8] in a one-dimensional approximation. The theoretical models take cognizance of the scattering events by adopting a pair-creation length ℓ_{pair} and a phonon-scattering length ℓ_{phonon} which are, respectively, nominal electron "free paths" between pair-creation and phonon emission events. The terms are conveniently combined to give a reciprocal scattering length c,

$$c \equiv \frac{1}{\ell_{pair}} + \frac{1}{\ell_{phonon}}$$

Including the reflection term and a factor of 1/2 to account for the 50% probability that the electron is excited with a momentum component directed toward the surface, the probability that an electron reaches a surface x units away and does so without collision is simply,

$$P_o(x) = 1/2(1-R)\ \exp(-cx).$$

Recursive relations may be developed, giving the probability $P_n(x)$ that the electron reaches the surface after exactly n collisions. To obtain the average probability of escape Q by an excited electron, these P_n are summed $0 \leq n \leq \infty$. Berglund and Spicer[6] and Kane[7] conclude with similar expressions,[9]

$$Q = \frac{B\alpha}{\alpha + \mu},$$

where

$$\mu \equiv \sqrt{c^2 - a\ c},$$

$$B = \frac{(1-R)c}{(1-R)c + \mu(1+R)}.$$

The point to be emphasized here is neither the interpretation of B or μ, nor the details of the derivation; these are treated elsewhere. Rather, it is the appearance of the escape probability Q as a simple function of EUV absorption, phonon and pair-creation and surface reflection coefficient.

1.2 The Influence of Dislocations

We hypothesize that there will be, in a non-ideal crystal, scattering events due to the imperfect state of the crystalline lattice, and that, by analogy with the treatment of the ideal case, a scattering length ℓ_i can be ascribed to each type of event. Hence,

$$c \longrightarrow \frac{1}{\ell_{pair}} + \frac{1}{\ell_{phonon}} + \Sigma \frac{1}{\ell_i}.$$

The present work was begun on the premise that the dislocations within a photoemitter are the occasions for such scattering events, and that the photoelectric yield is changed thereby. The chemically unsaturated or "dangling" bonds along an edge dislocation certainly will be centers for inelastic scattering. The lattice discontinuities at both crystallite and grain boundaries partially reflect electron waves, scattering the electrons elastically. The former case will reduce the quantum yield while the sign of the latter effect is not predictable.

The quantum yield may be affected also by the presence of relatively open channels along grain boundaries. These would be too small to be "seen" by the radiation, since $\lambda \sim 1000$ Å, but would be large enough to increase the average electron free path. The most significant change would be produced by channels approximately normal to the emitting surface.

The yield may be affected in other ways. 1) The intersection of dislocations with the surface produces a micro-structure which may alter the effective work function, the reflectance ρ, and the electron reflection coefficient R. 2) Additional change in the work function will be produced by the presence of a strain field at the surface, as shown by Andreev and Palige,[10] Dillon and Oman,[11] Wainfan et al,[12] and Farnsworth and co-workers.[13-15]

The interplay of these factors will, in principle, affect both the yield and the energy distribution $dN(E)/dE$ of emitted electrons. This report summarizes observations of both yield and energy distributions for a number of metals with varying dislocation densities.

1.3 Energy Distribution of Photoelectrons

Spicer and co-workers[16-20] have shown the value of studying the energy distribution of photoelectrons (EDPE). Their studies were directed 1) toward an understanding of the photo-excitation process, and 2) measurement of the density of states in the valence and conduction bands of a number of materials.

The present work tests the hypotheses 1) that plastic deformation and the resultant generation of defects alter the quantum yield of a

photoemitter, and 2) that the EDPE is modified in a detectable way. We consider here the procedure to be followed in making EDPE observations.

When an effective retarding voltage V^* is applied between photoemitter and collector, only those electrons having energy $E \geq eV^*$ will reach the collector. Denote by N(E) the number of electrons with energy in the differential range between E and E + dE. The measured current is,

$$I(V^*) = e\int_{eV^*}^{\infty} N(E)dE.$$

Because the V^*-dependence enters as a result of the lower limit of integration, the derivative of $I(V^*)$ gives the EDPE,

$$-\frac{1}{e}\frac{dI}{dV^*} = N(eV^*) = N(E).$$

The effective retarding voltage V^* is the sum of the true applied voltage and the contact potential difference between collector and emitter. Hence,

$$V^* \equiv V + \phi_c - \phi_E.$$

For accurate measurements of N(E), then, the difference $\phi_c - \phi_E$ must be known. This requirement points out the problems of dealing with 1) polycrystalline materials for which a range of ϕ's is present, 2) surfaces with an unknown state of contamination, and 3) surface contaminants whose concentration may be time-dependent. As is discussed below, it is clear that these circumstances were present and that they affected adversely our measurements.

EDPE analyses are ordinarily performed with retarding fields having plane, cylindrical, or spherical symmetry. However, the true energy distribution is measured only in a spherical retarding field, only if the emitting spot is at the center of symmetry, and only if it has a typical dimension much smaller than the emitter-collector separation. The last requirement is relaxed in a multiple grid system which permits both specimen and first grid to be operated at the same potential. This eliminates the electric field at the surface of the sample.

Nonetheless, plane-parallel geometry is employed frequently because it simplifies both construction and alignment. It is widely presumed

that a clear correlation exists between the EDPE's observed in this and in spherical geometry. There is surely a qualitative relation: one is on safe ground, for example, to observe that there will be fewer low-energy electrons in the true EDPE than in the plane- or cylindrical-symmetry EDPE. However, it is likewise clear that there is no unique analytical relation between such EDPE's: a variety of true EDPE's (i.e., measured in spherically-symmetric fields) can be prepared which will produce a single apparent EDPE (i.e., measured in non-spherically symmetric retarding fields).

Hence, the potential benefits of using plane-parallel geometry for EDPE analyses must be appraised with caution. For preliminary work, this geometry suffices to reveal qualitative differences in EDPE's; quantitative measurements, which lead to an attribution of EDPE differences to specific mechanisms, must be performed in spherically-symmetric retarding fields.

2 EXPERIMENTAL PROCEDURES

2.1 Specimen Preparation

Table 1 summarizes the essential facts of specimen purity, annealing, deformation, and surface preparation. Not indicated are the details of mechanical polishing for which a standard selection of decreasing grit size was employed, the last step being a polish with 0.5μm alumina on felt.

A pre-deformation anneal insured that all specimens were initially without residual strains. Annealing temperatures were chosen to be about 65-75% of the melting temperatures except for the Mo specimens. In this case caution in annealing furnace use prohibited temperature in excess of 1300°C--about 55% of the Mo melting temperature. Nonetheless, the Mo samples were expected to anneal fully in five hours' time.

Before each experiment with a given sample, its surface was etched as indicated. (In one set of experiments on Fe, two etchants were alternated and produced the results discussed in Section 3). Suitable rinses followed, the samples were dried in a hot air blast, and were mounted in the monochromator exit chamber, behind and coaxial with the various beam-defining slits.

Table 2 lists the characteristics of each of the twenty-eight specimens. The first entry is always the unstrained sample. The strain ε is calculated directly from the ratios of initial to compressed thicknesses, ℓ_o and ℓ:

$$\varepsilon = \log_e(\ell_o/\ell).$$

Hence, a specimen for which the thickness has been reduced to 50% of its original value would have been strained, in compression, by $\varepsilon = 0.69$.

The grain size is taken as the average grain dimension, determined by optical microscopy of the etched specimens. This measurement is distinguished from that of the average crystallite size. The latter is performed by x-ray line-broadening analysis,[22] and its result is representative of the scale over which true crystalline order is maintained.

TABLE 1

SPECIMEN PREPARATION

Sample	NICKEL	IRON	MOLYBDENUM	ALUMINUM	COPPER
Source	MRC-VP Grade	MRC-VP Grade	MRC-VP Grade	MRC-MARZ Grade	Commercial OFHC
Nom. Purity	99.99%	99.95%	99.95%	99.999%	----
Principle Impurities (by wght)	C 50ppm O 20 Cu 15	O 78ppm Mo <50 Cu 50 Sn 40 Si 35 S 30	W 50ppm Si 25 Mg 20 Cr 15 Cu 15	C 5ppm O 5 Zn 1	
Anneal:					
Pressure	5×10^{-5} torr	4×10^{-5}	3×10^{-5}	5×10^{-5} torr	3×10^{-6}
Temperature	1090°C	1100°C	1300	300°C	750°C
Duration	5 hrs.	5 hrs.	5 hrs.	5 hrs.	5 hrs.
Deformation	$0 \leq \varepsilon \leq 1.00$	$0 \leq \varepsilon \leq 1.00$	$0 \leq \varepsilon \leq 0.70$	$0 \leq \varepsilon \leq 1.37$	$0 \leq \varepsilon \leq 0.40$
Etchant	HNO_3:Acetic: Acetone 1:1:1	H_2O:HNO_3 1:1	HCl:H_2O_2 1:1	NaOH (dilute)	

TABLE 2

STRUCTURAL CHARACTERISTICS OF PHOTOEMITTERS FROM DIFFRACTOMETER LINE-BROADENING ANALYSIS

Sample	Strain (Compression)	Grain Size	Crystallite Size	Lattice Strain	Dislocation Density
Fe_1	0	44 μm	7.741 μm	0 X 10^{-3}	5.0 X 10^{6} cm^{-2}
Fe_2	0.10	↓	4.054	0.14	18.2
Fe_3	0.25		1.776	0.68	9.4
Fe_4	0.45		-	0.96	-
Fe_5	0.70		-	1.03	-
Fe_6	1.00		-	1.15	-
Ni_1	0	500 μm	7.77 μm	0 X 10^{-3}	0.049 X 10^{8} cm^{-2}
Ni_2	0.10	↓	0.630	0.65	7.55
Ni_3	0.25		0.522	0.85	11.0
Ni_4	0.45		0.351	0.93	24.3
Ni_5	0.70		0.270	0.86	41.2
Ni_6	1.00		0.230	1.03	56.7
Al_1	0	2.8 μm	0.430 μm	0 X 10^{-3}	1.64 X 10^{8} cm^{-2}
Al_2	0.10	↓	0.175	0.70	98.4
Al_3	0.25		0.144	0.80	144.
Al_4	0.45		0.123	1.07	197.
Al_5	0.70		0.086	0.80	403.
Al_6	1.00		0.084	0.97	421.
Mo_1	0	13 μm	2.552 μm	0 X 10^{-3}	0.46 X 10^{8} cm^{-2}
Mo_2	0.25	↓	1.130	0.70	2.35
Mo_3	0.45		0.896	0.90	3.74
Mo_4	0.70		0.627	1.05	7.61
Mo_5	1.00		0.168	1.22	105.
Cu_1	0	550 μm	-	-	-
Cu_2	0.11	↓	-	-	-
Cu_3	0.17		-	-	-
Cu_4	0.31		-	-	-
Cu_5	0.51		-	-	-

Hence, within a single grain, there are numerous crystallites separated from one another by low-angle grain boundaries. Whereas grain size is relatively independent of cold work, one expects--and measurements substantiate this--that the crystallite density will decrease rapidly as the samples are strained.

The line-broadening measurements were performed on a General Electric XRD-5 x-ray unit, including diffractometer, using Cu K-radiation at room temperature.[22] Calculation of crystallite size and dislocation density were made using standard methods.[23-26]

The residual lattice strain $\Delta d/d$ follows immediately from the differential of Bragg's Law:

$$\Delta(\log n\lambda) = 0 = \Delta(2d \sin \Theta)$$

$$\frac{\Delta d}{d} = \frac{\Delta \Theta}{\tan \Theta} .$$

The experimental steps require that the angular width β at half maximum intensity of the diffraction line be determined and that they be corrected for instrumental broadening, the latter requiring line widths from a W powder sample. Then $\Delta\Theta = \beta/2$.

2.2 Instrumentation

All photoemission studies were performed in a 1-meter vacuum monochromator constructed by personnel of the Syracuse University Research Corporation, and schematically depicted in Figure 1. Radiation is produced in a Hinterreger type, high energy, vacuum ultraviolet discharge lamp.[27] This flow-through type lamp permits use of a variety of gases and mixtures of gases. Accordingly, one has a wide choice of line and continuous spectra. We confined our use to low pressure discharges in hydrogen and helium, and we employed the Lyman-α radiation from each--1216 and 584 Å respectively.

There could be no "window" between lamp and monochromator because all materials are opaque in the vacuum ultraviolet below 1050 Å. To prevent

C9392

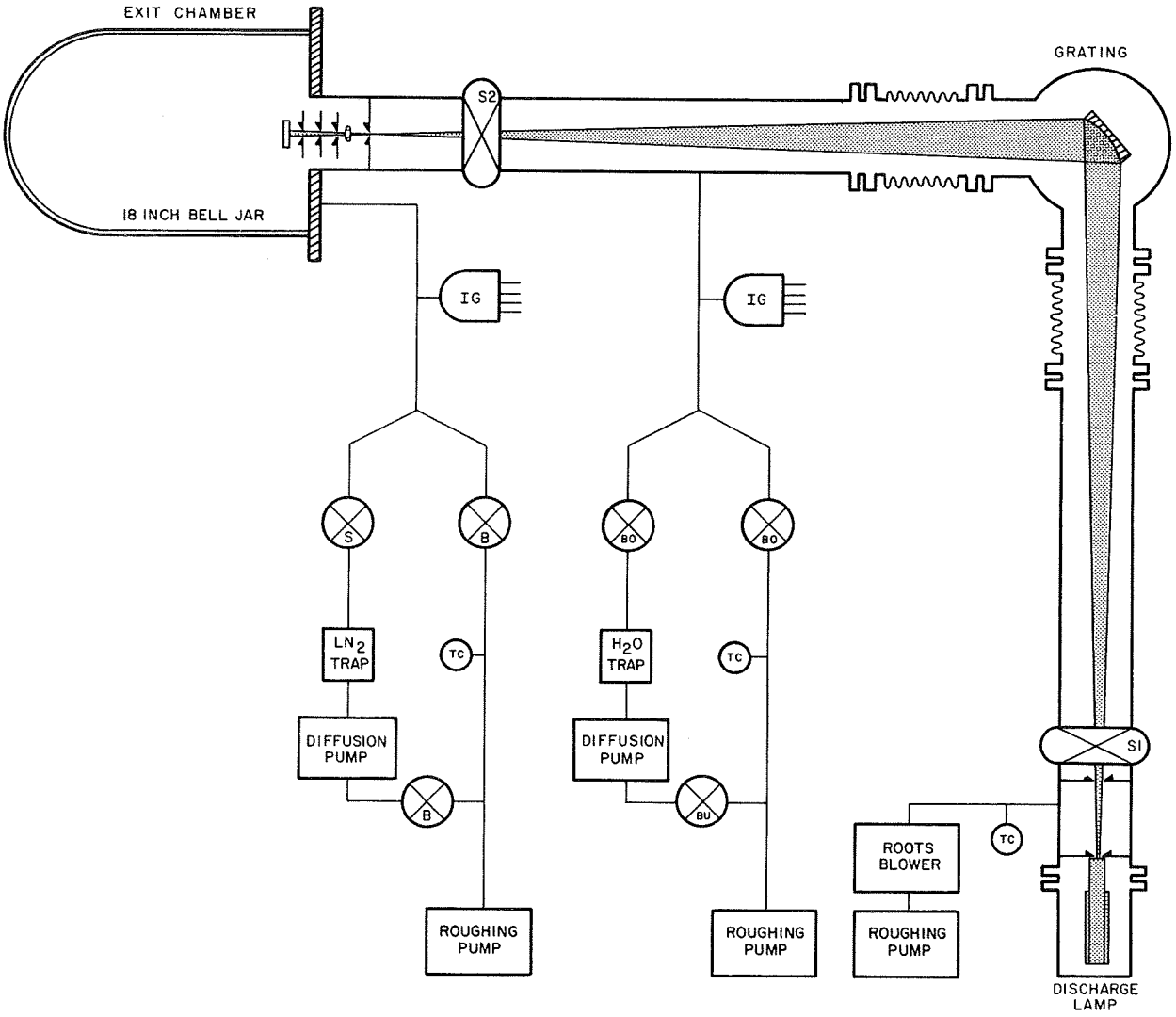

FIG. 1--SURC EXTREME ULTRAVIOLET MONOCHROMATOR - SCHEMATIC.

discharge-lamp gas from entering the main monochromator chamber, a differential-pumping chamber separated the lamp from the monochromator. The combination of a Roots blower and roughing pump maintained the pressure at 10^{-4} torr in this intermediate chamber. The main chamber pressure is reduced to $\sim 10^{-5}$ torr by a water-baffeled, silicone-oil diffusion pump. This chamber may be isolated from the differential chamber by slide valve S1.

The concave diffraction grating is 40 x 80 mm in size, bipartite ruled at 1200 lines/mm, and blazed for 800 Å (in first order). Incident and diffraction angles are nominally 45°, giving a reciprocal linear dispersion ("plate factor") of 5.8 Å/mm at the variable-width exit slit.

The synchronous drive which positions the grating is not calibrated in terms such as wavelength versus angle, with the result that reliable operations are confined to the few very strong lines in the characteristic spectra of each gas. In the context of the present experiment, this is not a major drawback since photocurrents are measured by an electrometer which is useful to about 10^{-14} amp. Only the strongest and most readily identified lines supply photon fluxes large enough to produce currents of this magnitude. If electron multiplication techniques were being used, weak, continuous spectra could be employed and then accurate wavelength versus positioning information would become requisite.

Flexible sections in the monochromator arms permit the correction of misalignments; other such sections (not shown) isolate the chamber from vibrations caused by the roughing pumps and other sources.

The monochromator terminates in the exit chamber, an 18" diameter bell jar which is separately evacuated and may be isolated from the monochromator by the slide valve S2. Additional valves isolate the liquid-nitrogen-trapped diffusion pump from the exit chamber when the latter is open to air. Exit chamber pressures are typically 10^{-5} to 10^{-6} torr. Specimens are mounted in insulated holders supported by nylon fasteners screwed into the bell-jar base plate.

Details of the various beam-defining slits in the exit chamber are shown in Figure 2. The exit slit is approximately 0.500" x .020" and variable in width. Beyond the exit slit, the beam is partially intercepted by a .300" loop of copper wire, producing, under EUV illumination, a

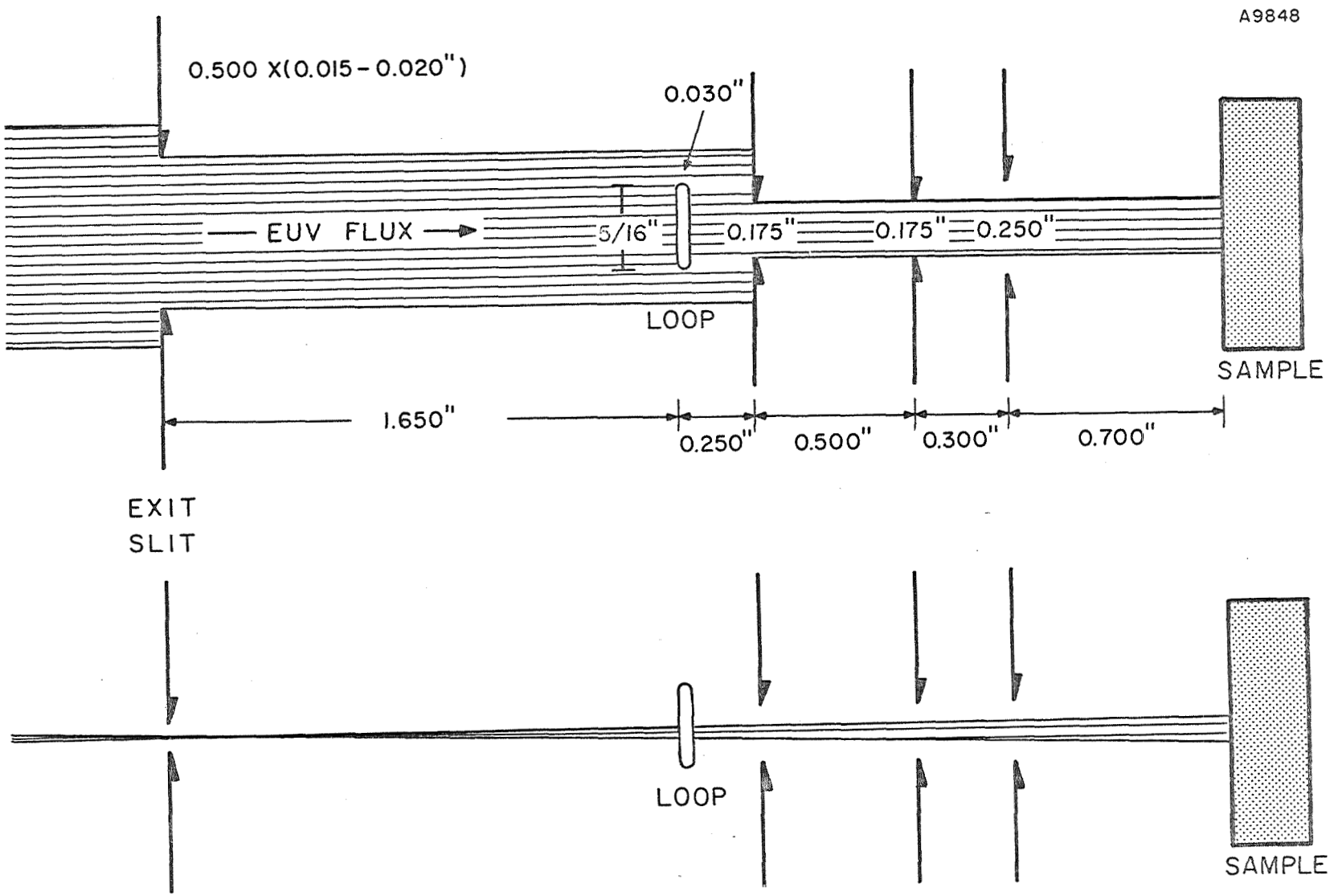

FIG. 2--DETAILS OF EXIT CHAMBER GEOMETRY.

current of photoelectrons--the "loop current". The inner diameter of the loop is sufficiently larger than the diameter of the next apertures--0.240" compared to 0.175"--that the EUV flux to the sample is independent of the precise alignment of exit slit and loop. Hence, the loop current is a monitor of the EUV flux to the sample. For measurements of relative photoemission yield, it is required only that the combination of lamp power and slit widths be adjusted to produce a predetermined, fixed loop current.

Absolute intensity measurements of EUV flux, which would be needed if quantum yield--photoelectrons/incident photon--were desired, require a device such as a gas photoionization detector, or a detector calibrated against such a standard.

The final collimating aperture is made somewhat larger than the two preceding ones to insure that there are no photoelectrons produced at its peripherary. Such electrons, if generated, would confuse the retarding field measurements. There is always a small reverse current, however, observed under deep retarding conditions ($eV > h\nu - e\phi$) where no current at all is expected. It is ascribed to photoelectrons produced at the collector plate by reflected photons and drawn to the specimen by the applied field (which is a retarding field for electrons produced at the specimen).

Figure 3 is a block diagram and schematic of the photoemission study instrumentation. Photocurrents are measured by the sample picoammeter,[28] displayed by a digital voltmeter (DVM),[29] and recorded by a printer[30] operating at up to 5 lines/second.

The potential of the accelerator plate is determined by the resistance-programmed retarding voltage source.[31] A positive voltage with respect to the specimen draws the maximum or "saturation" current. A negative potential V permits collection of only those electrons with kinetic energy $E_{kin} \geq e(V+\overline{\phi}_c-\overline{\phi}_E)$, as noted in the introductory section. A decade resistance box connected to the appropriate terminals of the voltage source determine the applied voltage. The 1 mv/Ω programming constant was found to be quite stable, and the desired voltage points could be reproduced quickly and accurately.

The DVM-printer combination, used principally to display and record sample picoammeter readings, may be switched to monitor also the loop

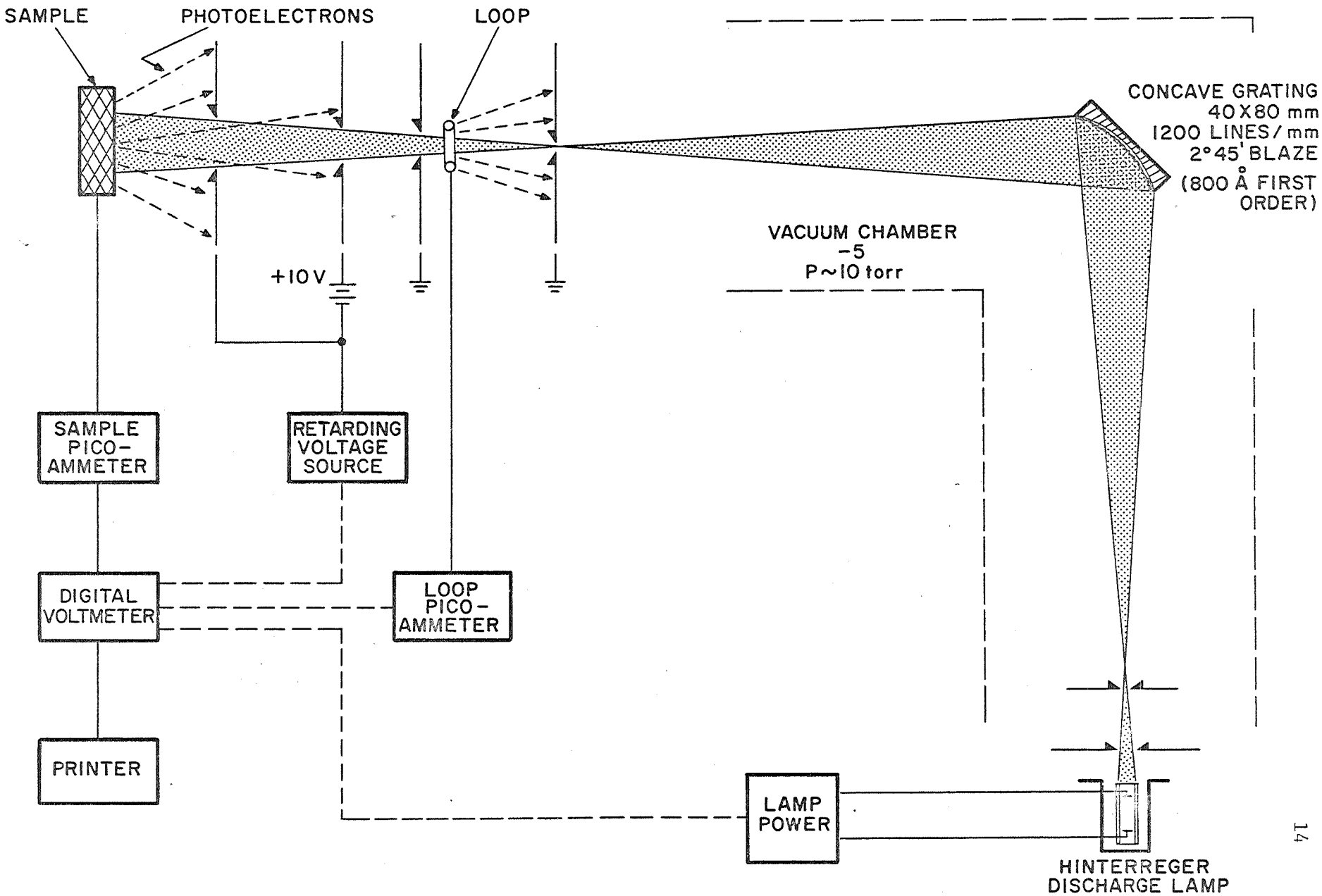

FIG. 3--PHOTOEMISSION STUDY - SCHEMATIC.

picoammeter, the retarding voltage and the discharge lamp current. A record of these variables is quite desirable in reconstructing all conditions pertinent to a given experiment. Not indicated in Figure 3 is the optional DVM connection to an ionization gauge controller, the latter being used to measure exit chamber pressures.

2.3 Conduct of the Experiment

The preparation and characterization of specimens has been described above. This section details the step-by-step routine of each experiment or "run".

The surface of each sample was etched immediately prior to a study of its properties. The advantage in this, beginning an experiment with the same nominal state of "contamination", was offset somewhat by the possibility that variations in surface reflectance from etch to etch would exist in a given sample. In all cases, the surfaces exhibited a very uniform and fine-grained appearance. This will be observed in some of the photographs of Figure 4. We did not assess the extent of topographical variations from run to run.

When the exit chamber was open to allow mounting of a new sample, the monochromator proper was valved off, and the EUV discharge lamp was kept running. Once the bell jar was repositioned and vacuum pump-down started, it was a matter of a few minutes only before the first observations could begin. Overall "turnaround" time was about 15 minutes.

The first measurements were made at this time, primarily to observe effects of the sample's initial outgassing and subsequent adsorption of contaminants from the vacuum ambient. The former was due to the desorption of surface films which had been picked up by the sample during exposure to air before evacuation; the latter is thought to be due to the residual pressure of the silicone pump-oil, among other things. Generally, the yield drifted upward, rapidly at first, but gradually slowing with time. After twelve hours, the apparent drift was reduced to less than 1% per hour. Since possible systematic drifts of this magnitude may have been present in current-measuring circuit, this level of apparent drift was

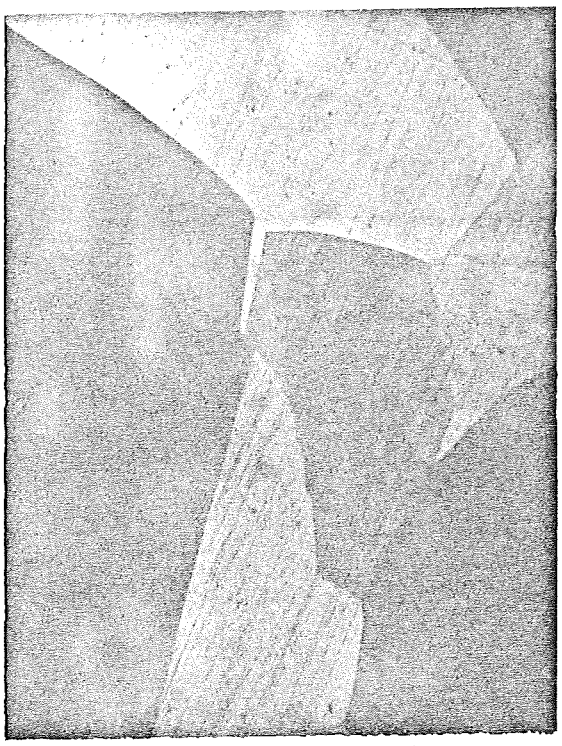

100 μm

NICKEL

100 μm

COPPER

100 μm

IRON

100 μm

MOLYBDENUM

FIG. 4--TYPICAL GRAIN STRUCTURE OF NI, CU, FE, AND MO SAMPLES.

arbitrarily designated as a "steady state" condition, and the final measurements were taken at that time. The overall drift frequently ranged between 15 and 20% of the initial value.

Two types of measurements were involved: yield and EDPE (energy distribution of photoelectrons). Although yield may have varied with time, the normalized EDPE did not change. Hence, the former was measured much more frequently than the latter.

The final measurements typically concluded a series of retarding runs, each of which involved current measurements at 70-80 values of the retarding potentials. All measurements were repeated. These runs were performed during the drift period and, except for the slowly changing magnitude of the measured currents, they did not differ at all from one another. That is to say, the normalized retarding runs were identical both during and at the end of the drift period.

A computer handled the large amounts of data, performing simple but highly repetitive averaging and normalizing steps. It was interfaced with a plotter, and the combination acted to give normalized graphs of I(V) and dI(V)/dV. A tracing of the typical output is shown in Figure 5. The solid line is a graph of the measured current values. These values were entered with the assumption that four-figure relative accuracy existed. The repeatability of current data points to better than one part in a thousand supports this assumption. In the most interesting region, between +1.00 and -5.00 volts, the increments in collector potential were 100 mv.

The dashed line of Figure 5 is the slope of the retarding curve, that is, the average current in a given interval plotted at the center of that interval. The succession of small peaks and valleys noted particularly in the negative tail of the derivative curve appears just as the measured currents drop below $.1000 \times 10^{-12}$ amp, and the data contains three figures only. (We found it desirable to remain on the same scale for all measurements because the overlap of successive decades was not satisfactory and also because of the long time constants involved with using the next highest input resistor.) Earlier runs, which were programmed to three figures only, showed this "noise" beginning much earlier and becoming much larger in amplitude than in the present case. Both observations underscore the need for high relative accuracy in measuring these retarding

curves. Obviously the accuracy of yield measurements, which involve the ratio of absolute current measurements, is limited to $\sim$ 3% by the electrometer accuracy.

Not all studies were done in this way since much information could be obtained directly from a hand-plot of the data. This was most conveniently done in semi-logarithmic coordinates, as shown in Figure 6, where the logarithm of the collected current is plotted as a function of the collector potential. As this potential becomes more negative with respect to the photoemitter, increasingly fewer photoelectrons have sufficient energy to reach the collector.

The indicated correction to collected current is attributed to electrons generated at the collector by reflected photons. In the present case the reverse current was $I_R = -0.040 \times 10^{-12}$amp, though it has been observed to be as high as -0.200×10^{-12}amp for other samples. Once the measured data (open circles) are augmented by I_R, the corrected data (solid circles) are plotted and a straight line drawn tangent to the general trend of data. It is not clear that the slope of this line has any physical meaning, as it does, for example, in a retarding field thermionic emission experiment where the absolute temperature $T = (e/k)\ dV/d(\log I)$; but the slope has proven to be a useful quantity in a number of cases, as described below.

The slope of the true retarding line (i.e., the data plotted in linear coordinates) gives the apparent EDPE (energy distribution of photoelectrons), $N^*(E)$. In the present case it is clear that

$$N^*(E) \quad \alpha \quad \exp(-\beta V)$$

where β is some constant. Qualitatively, the larger the value of β, the smaller is the extent to which higher-energy electrons are present in the distribution. If plastic deformation and the concomitant generation of crystal defects serve as mechanisms for increasing inelastic scattering events, these effects are expected to appear, both as a changed value for β as well as in the EDPE.

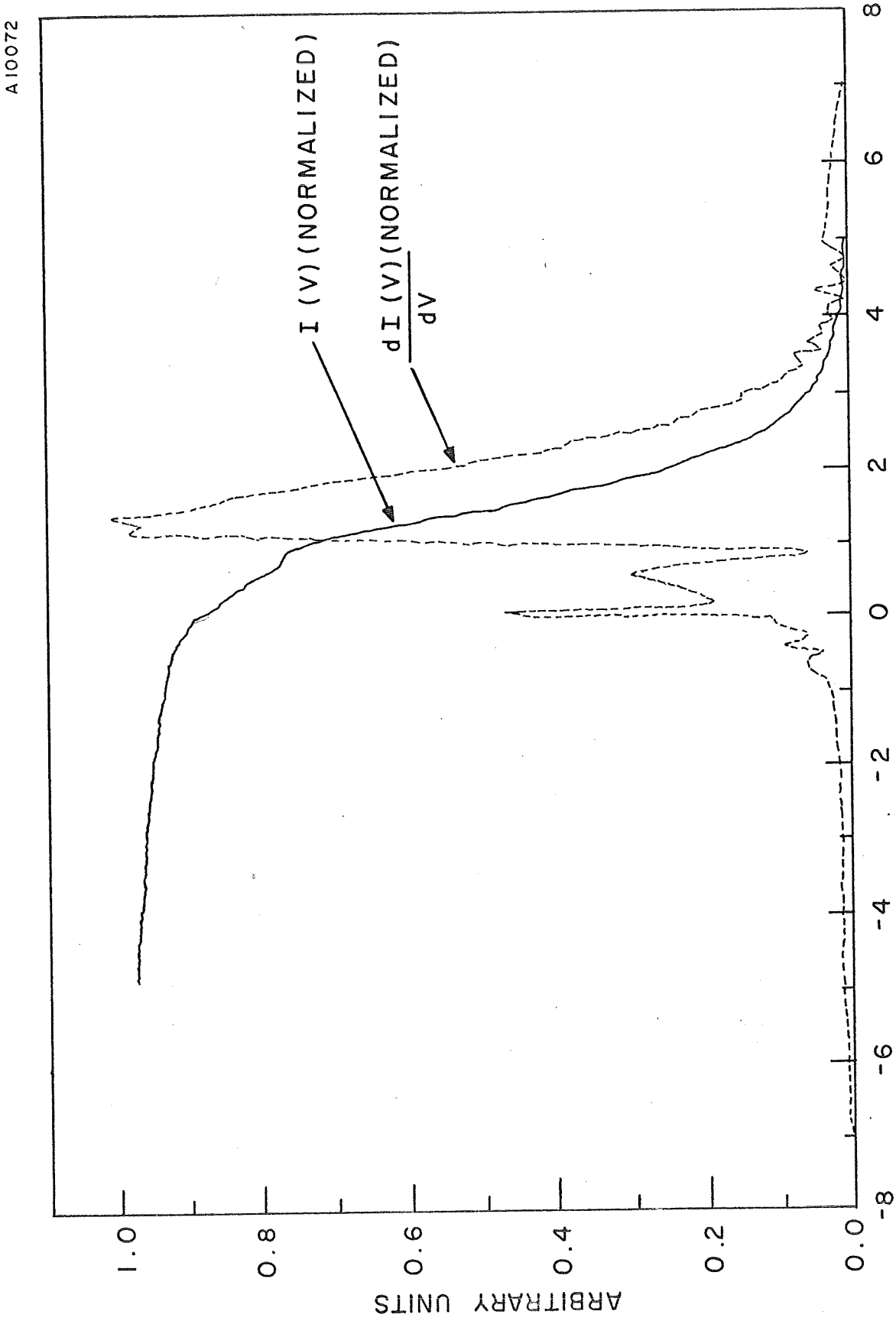

FIG. 5--TRACING OF PLOTTER OUTPUT OF I(V) AND dI(V)/dV.

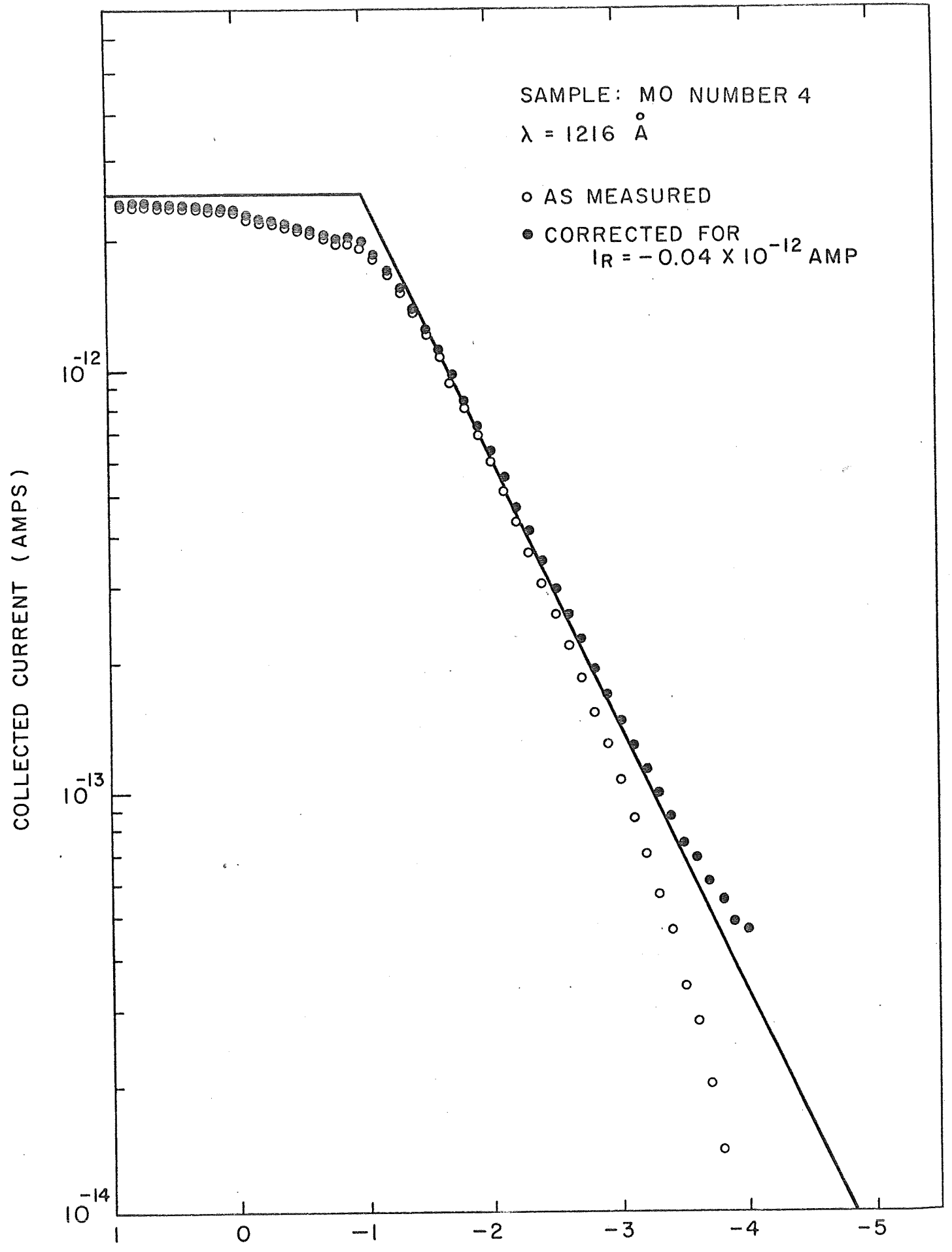

FIG. 6--TYPICAL SEMI-LOG PLOT OF RETARDED CURRENTS.

3 RESULTS

3.1 EDPE Measurements

Figure 7 shows that $\beta(Al)$ is quite insensitive to the extent of plastic deformation. The small scatter in $\beta(Al)$ may be attributed to imprecise measurement of reverse currents and to the general arbitrariness involved in drawing a tangent line to the retarding plot.

A wholly new situation developed for $\beta(Mo)$, as shown in Figure 8. Here, β tends toward successively higher values with increasing plastic deformation. The trend is not monotonic since $\beta(Mo_4) > \beta(Mo_5)$, but the strong suggestion remains, nonetheless, that an increase of defect dendity in Mo leads to a decrease in the relative numbers of high-energy photoelectrons. Although the reasons advanced to explain the scatter in $\beta(Al)$ apply in the present case, neither uncertainty in drawing the best β-line nor the uncertainty in determining the reverse current correction significantly alter the position and slopes of the $\beta(Mo)$ lines. This much is clear from Figure 6. The conclusion: deformation has surely altered the high energy side of the Mo EDPE, and in such a way as to reduce the relative numbers of higher-energy electrons.

Similar experimentation has been conducted using Cu, Fe and Ni samples. The β-plot for these show scatter similar to the Al results.

Hence, these investigations reveal that photoemission from Mo, alone among the five materials studied to date, clearly evidences mechanisms which affect the EDPE. Changes in the EDPE are correlated with dislocation density in the Mo case.

3.2 Yield Measurements

Figures 9 and 10 summarize our observations of the dependence of yield upon both wavelength and true strain (alternatively, defect concentration). As described earlier, the plotted points are the ratios of maximum sample current to loop current, both measured at the end of a suitable drift period.

A9944

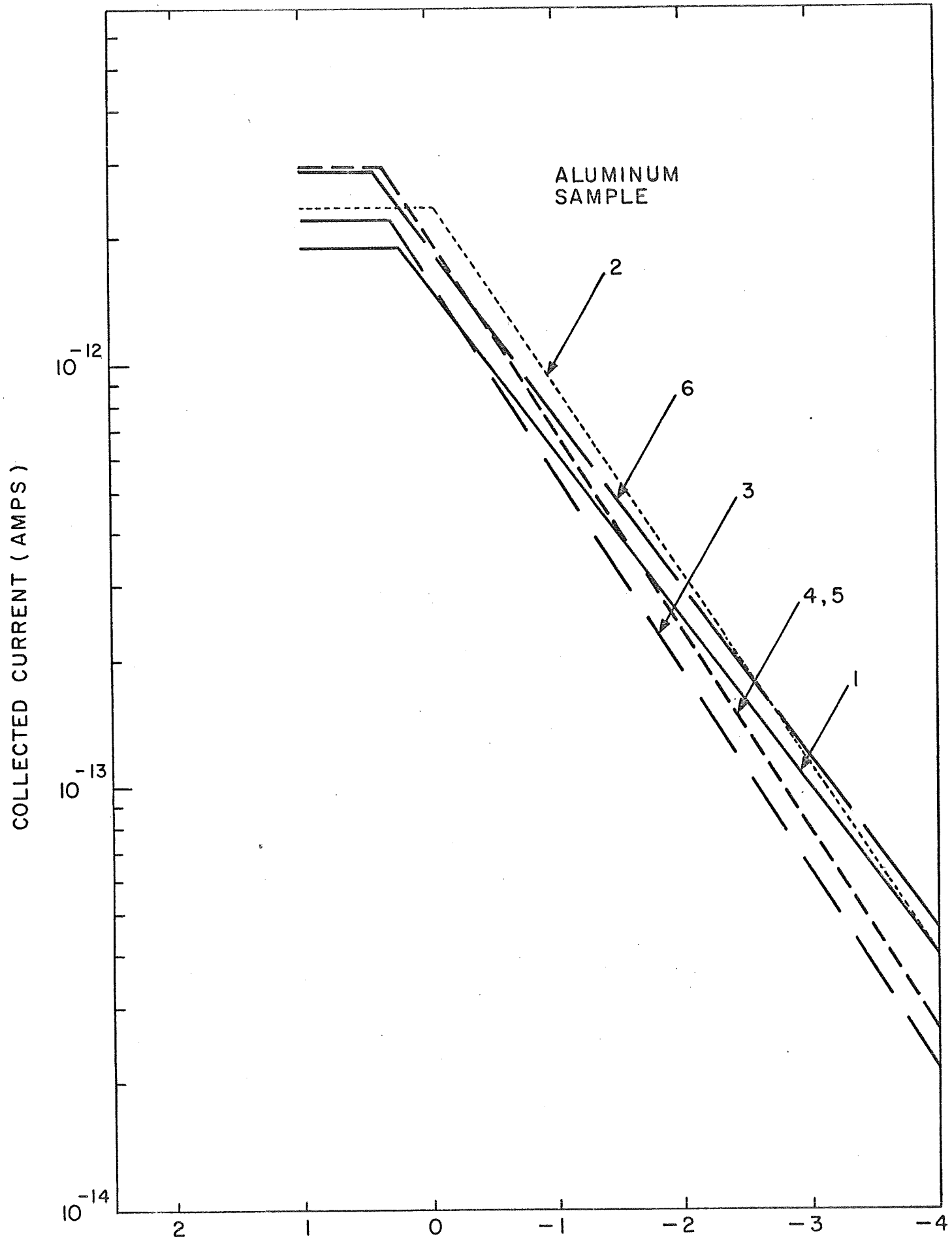

FIG. 7--RETARDING PLOTS FOR SIX ALUMINUM SAMPLES.

A9945

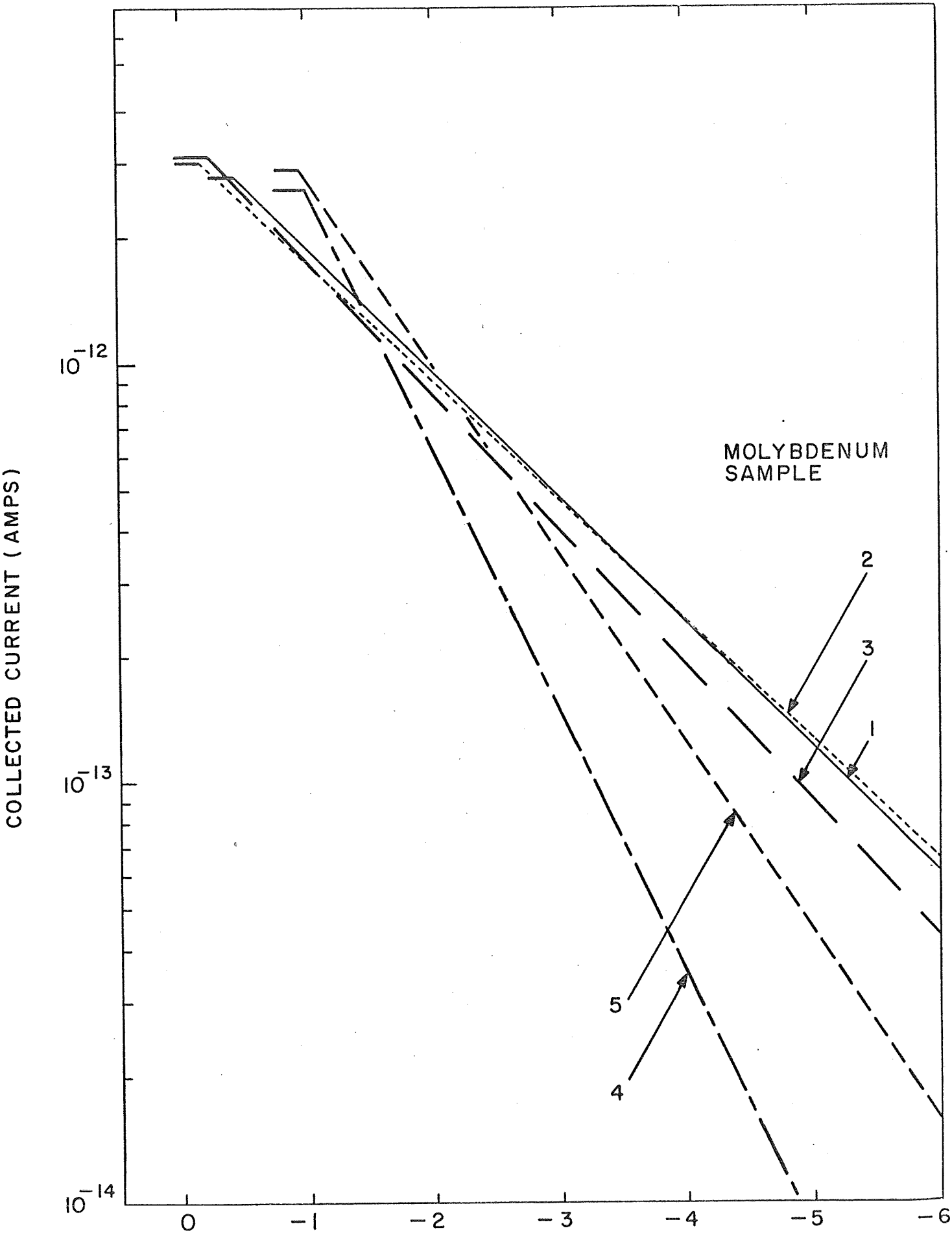

FIG. 8--RETARDING PLOTS FOR FIVE MOLYBDENUM SAMPLES.

The scatter, which is obviously present here, obscures nearly all but the fact that there are no yields strongly dependent on strain, with the exception of Al at 1216 Å, and possibly Ni at 1216 Å. No change at all of yield with strain can be claimed for Fe(584), Fe(1216), Cu(584), Cu(1216), Mo(1216, or Ni(584). The yield of Al(584) was found to be slightly strain-dependent.

A smooth curve has been fitted to each set of observations, with varying degrees of reliability. The widest scatter is present in the Ni(1216) results, and the line drawn there is indeed extremely arbitrary. Its significance does not extend beyond the observation that there seems to be a downward trend, perhaps monotonic, of yield with strain.

The data scatter reflects also on the difficulty experienced in dealing with Ni in the present experiment. The Ni samples were found consistently to exhibit the largest and least predictable drifts. Given the popularity of Ni targets in photoemission work, further investigation of the strain-dependence of the Ni yield is surely indicated.

The correlation between a decreasing yield and an increasing strain for Al(584) is readily apparent. What is not clear, though, is whether the relation is best described as linear, as suggested by the fit to the initial set of data (open circles), or whether it is exponential, as suggested by the fit to a set of experiments (solid circles) performed much later in the course of the program. Perhaps both trends exist and the measured trend depends simply on which patch or combination of patches are being studied. It has been noted earlier that these experiments were performed with polycrystalline samples and without strict control of the sample area being irradiated.

The two sets of Al(584) were separated by some weeks of experimentation on other samples. Though it is not clear why the repetition points lie systematically below the initial points, both for Al(584) and more obviously for Fe(584), the following could explain the change: It is speculated that the loop sensitivity increased during the course of the experiments. Since all measurements are referenced to a standard loop current, an increased sensitivity would lead the experimenter to reduce the EUV flux in order to return to the standard current. With an unchanged sample sensitivity, this would mean a reduced photo-current,

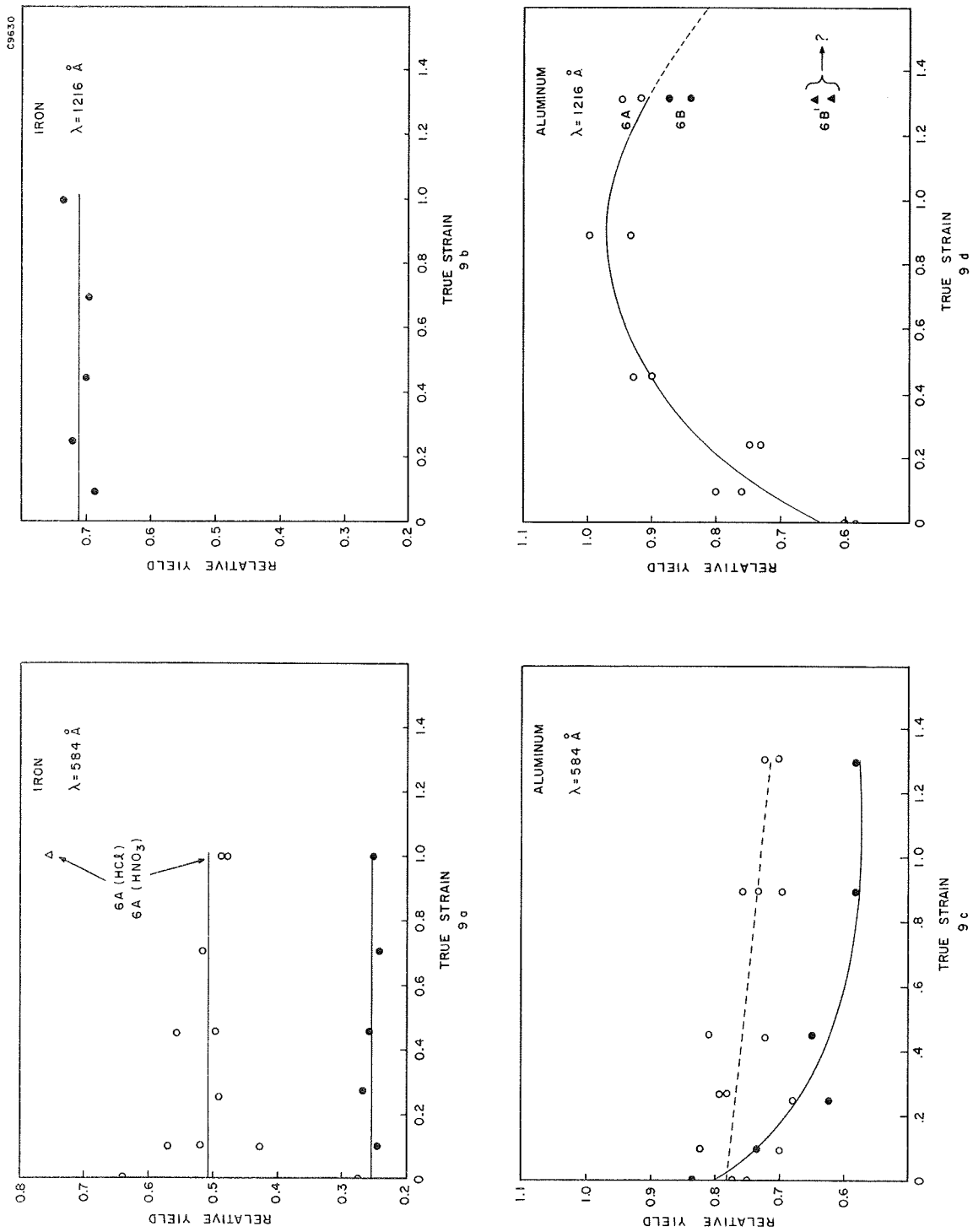

FIG. 9--RELATIVE PHOTOELECTRIC YIELDS OF IRON AND ALUMINUM AT 584 Å AND 1216 Å.

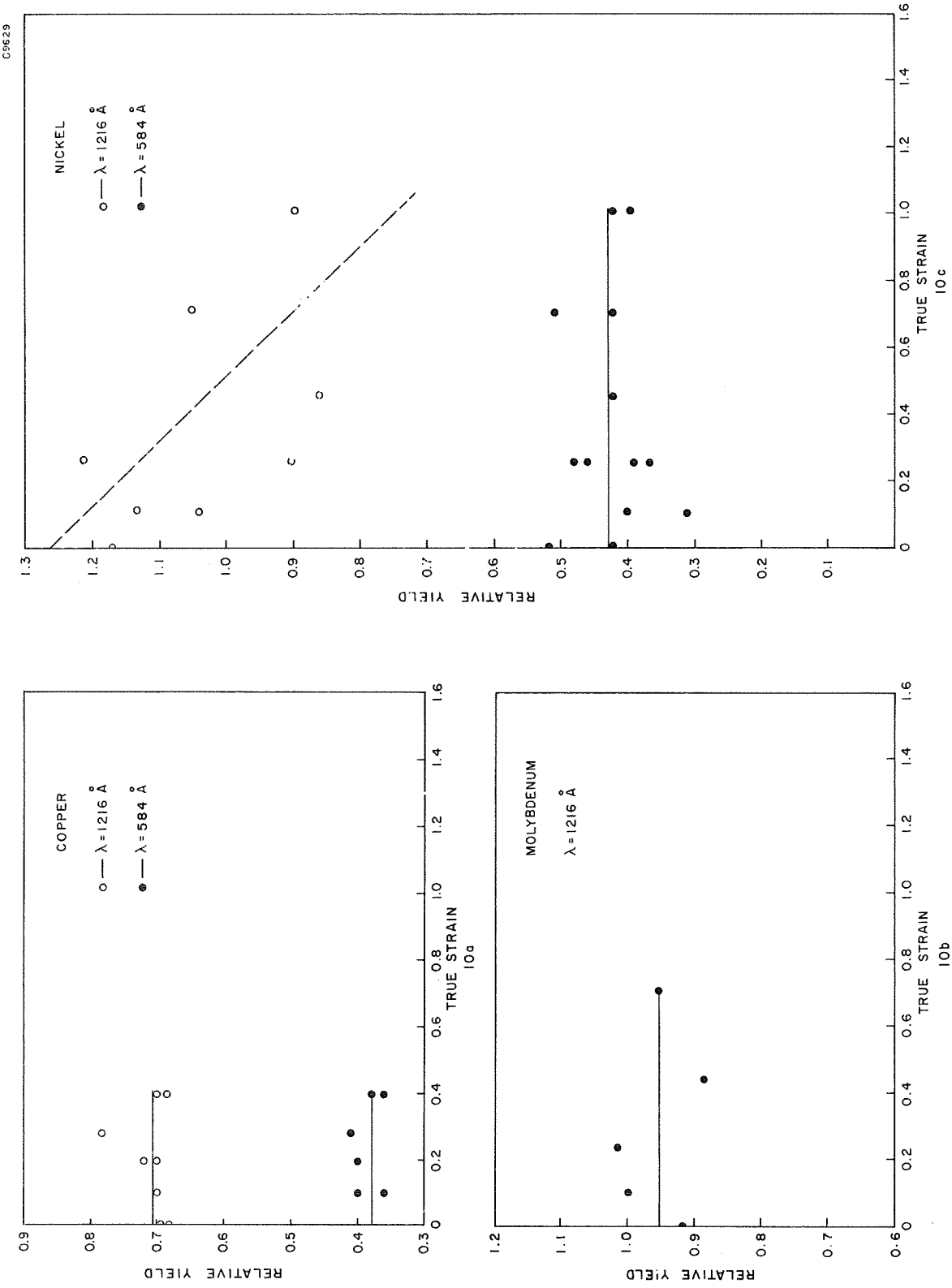

FIG. 10--RELATIVE PHOTOELECTRIC YIELDS OF COPPER, MOLYBDENUM AND NICKEL AT 584 Å AND 1216 Å.

such as was observed. Decomposition of pump oil by an EUV beam is known to decrease the reflectivity of a diffraction grating,[32] and small layers of contamination can produce large changes in photoemissive properties.[33-35] The same effect operating on the loop would produce the putative increase in loop sensitivity. A more conventional means of monitoring EUV flux, such as a sodium-salicylate-covered window and a phototube detector, would eliminate this ambiguity.

The differences which may arise from patch structure alone are suggested by an experiment performed Al sample #6 at 1216 Å, i.e, $Al_6(1216)$. This sample was sliced into two parts, Al_{6A} and Al_{6B}, just before the first experiment was undertaken. Samples Al_1 to Al_5 had already been examined. An experiment on Al_{6A} gave results indicated by the open circles of Figure 10b; the yield from the Al_{6B}, indicated by solid circles, was found clearly to be lower than the yield from Al_{6A}. Because the experiments were performed within 24 hours of one another, the possibility of drift in loop sensitivity, discussed above in connection with drops in the yields of Al(584) and Fe(584), seems to be excluded.

An experiment of a different kind followed this one. The surface of Al_{6B} was scored heavily with the blade of a penknife, re-etched, and restored to its mount in the monochromator exit chamber. The Al_{6B}, yield decreased by 25-30% and is plotted in Figure 10b as the solid triangles. Though the surface patch structure was undoubtedly changed by the gouging process, the primary effect is believed to have been a very severe, local cold-working and the generation of a much higher dislocation density than had existed previously. Hence, the triangle points should have been plotted at some higher value of true strain, though this value was unknown.

The yield vs. strain curve exhibited a maximum solely in the case of Al(1216). This is not clear if the data of Al_1-Al_{6A} only are considered. However, the Al_{6B} measurements must be regarded as weighted equally with those of Al_{6A}. Moreover, if the assumption about the state of cold work existing in the near-surface region of Al_{6B}, is correct, then there is additional strong evidence that a maximum in the yield-strain curve occurred near True Strain = 0.8. At this value one then obtains the maximum photoemission yield from Al.

The results of a series of measurements on sample Fe_6 are evidence of one complication of this experiment in its present form. The measurements on six Fe samples at 584 Å were preceded uniformly by etching each surface in an HNO_3 solution and thoroughly rinsing each with tap water. The data are summarized in the open circles of Figure 9a.

To investigate the possible extent of problems due to choice of an etchant, measurements were then performed on both sides of Fe_6, alternating NHO_3 and HCl etchants between runs. The observations are summarized in Table 3 and show clearly that the HCl etch resulted in higher yields. The enhancements were approximately 1.5 and 1.2 times for sides A and B, respectively.

TABLE 3

DEPENDENCE ON ETCHANT OF RELATIVE PHOTOELECTRIC YIELD; IRON (SAMPLE 6) IRRADIATED AT 584 Å

Sample	Etch	Yield
Fe_{6A}	HNO_3	51 %
	HCl	76
Fe_{6B}	HCl	73 %
	HNO_3	58
	HCl	70

We ascribe the yield changes to the formation of insoluble surface layers in one or both cases. Other sources of difference, a change in topography resulting in changed reflectance for example, are potential problems, but we view them as considerably less effective than varying surface layers in affecting the yields of the iron samples.

Unwanted layers are the bane of workers investigating surface properties of materials. They surely affect photoemission, and we believe

the evidence here clearly shows the sort of problems facing this experiment at present. Certainly both improved vacuum conditions (ca. 10^{-9}torr) and provision for heating samples in situ must precede any further studies. Otherwise, the influence of uncontrolled surface layers will continue to prevent full and satisfactory interpretation of results.

4 DISCUSSION OF RESULTS

The experimental program described here is the first reported attempt at correlating changes in both photoelectric yield and the energy distribution of photoelectrons (EDPE) with the dislocation density existing in samples of Cu, Fe, Mo, Al, and Ni. Hence, we can make no direct comparison of the overall results of this work with those of other programs.

There is the work of Veerman,[36] however, which does bear somewhat on our observations of Al and Fe yields. He operated in the near ultraviolet where mirrors, lens, etc. can be used to direct and focus the radiation. By means of mirrors oscillating about orthogonal axes, a focussed UV beam was swept across the surfaces of Al samples, successively illuminating all portions of a rectangular area. The resultant photoemission was detected and synchronously displayed on the screen of a storage oscilloscope. The result was a raster having a three dimensional appearance. Deviations from a raster of strictly parallel lines (which would be the result of no photoemission or, at most, constant photoemission) were due to local variations of the photoelectric response to the UV beam. Using this approach he was able to detect and display scratches, cracks and, most interestingly, the strain field preceding an advancing crack.

In another arrangement, specimens could be strained in tension. He observed that the photoemissive yields of Fe and Al increase with plastic deformations for deformations of up to 20%. There is no data beyond this. Hence, these results support the initial upward trend of our results for Al(1216), but do not go far enough to comment on the reality of the observed maxima in the strain-dependent yield of Al(1216).

The Fe samples were strained step by step. Each strain produced an increase of photoemission, but this decayed rapidly toward the level observed at time zero. The effect seemed to be due 1) to the generation of a fresh surface during strain, followed by 2) the contamination of this surface by adsorption from the ambient. Our failure to observe a strain-dependent photoelectric yield in Fe, to judge by the preceding evidence, is a result of our having prepared the samples in air and having

made no provision for generating fresh surface area (by cleaning or by straining, as Veerman did).

There are two particular areas which suggest comparison with other work, but the suggestions are misleading. 1) The Cu EDPE measurements performed by Berglund and Spicer[6] cannot be compared with the present work because of the differences in retarding field geometry: theirs was spherically symmetric whereas ours possessed plane-parallel symmetry. As discussed above, there is no necessary relation between observations performed with the two arrangements. 2) An attempt to draw conclusions about the wavelength dependence of quantum yield for the various materials is likewise fruitless. There was no provision here for measuring absolutely the incident EUV flux, nor for estimating the numbers of electrons produced per absorbed photon. This limitation and the one described in the preceding paragraph must be removed before further work is undertaken.

Two qualitative results stand out as the basis for further investigations of this type. The maximum in the strain-yield curve for Al(1216), once verified by other experiments, holds promise for new understanding of the fundamental role of dislocations in EUV photoemission. Also, the wide range of slopes of EDPE plots ("β-plots") signals the presence of other phenomena which are not understood and so are intriguing from a fundamental point of view.

There is practical interest here, too. A number of EUV radiometers have been flown into the upper atmosphere in a NASA-supported study of the EUV flux in the geocorona.[37-40] These radiometers rely on the photoemission and energy analysis of electrons from an Ag target. The incident radiation is a composite of a number of wavelengths, of course; hence, the observed EDPE is a composite function of the strength of the various lines and the sensitivity of the photoemitter to these radiations. The observed EDPE is analyzed in the laboratory into the sum of various wavelength-dependent EDPE's in a manner which relies on the prior calibration of the radiometer at each of approximately four principle lines. The procedure makes obvious assumptions about the detector stability and spectral sensitivity. It also relies on the near-uniqueness of each of the EDPE's. Our results with the Mo(1216) β-plots suggest that one may be able to tailor a Mo target, by deforming it plastically, in a way which would optimize the process of unravelling the various contributions to the observed, composite EDPE.

5 SUMMARY

This work has been successful as an exploratory program. In spite of experimental limitations, we have been able to identify anomalies in the Mo β-plots and to observe that the yields from Al and Ni are strain-dependent, while those from Fe, Cu and Mo appear to be relatively constant. These points have been discussed above.

Here we wish to draw together those aspects of improvement in experimental approach which are needed to improve the reliability of the data.

1.) There must be guarantees that the surface of each sample can be prepared in a repeatable way. This means, in particular, that all samples be cleaned in situ. The difficulties of relying solely on an etch prior to mounting and evacuation have been illustrated by the problems with Fe(584).

2.) If the samples are to be cleaned in situ, one must then have sufficient time to perform experiments. Since a full layer of contamination is deposited in one second at 10^{-6} torr (our present vacuum level), it is imperative that additional stages of differential pumping be added and that ultra high vacuum techniques be introduced to insure a vacuum of at least 10^{-9} torr in the EUV exit chamber.

3.) Necessary modifications must be made to facilitate absolute measurements of EUV flux. This would mean an ionization chamber and/or sodium salicylate window plus photomultiplier.

4.) The retarding field should be changed to one with spherical symmetry so that true EDPE's may be measured, and so that they can be compared with published spectra. The widespread use of multiple, hemispherical grids in low-energy electron diffraction (LEED) and Auger spectroscopy has resulted in standard versions of these becoming commercially available.

5.) The extent to which polycrystalline effects influence practical use of photoelectron devices should be investigated by studying the properties of single crystal targets.

6.) Two-dimensional scanning of surfaces should be implemented by use of appropriate positioning and motion devices. One then could verify the uniformity of yield from a sample which had been strained homogeneously. Following this, specimens could be strained in a known, but non-uniform manner, opening the way for studying a continuous range of strain and surface conditions existing in a single specimen. The latter would be highly desirable in an ultra high vacuum context where "turn-around time" becomes a matter of days rather than hours.

7.) Once the exploratory stages are effectively completed, specimens of particular interest could then be examined using, alone or in combination, a wide variety of techniques: LEED, Auger spectroscopy, ellipsometry, for examples.

8.) One could begin moving toward "practical" surfaces by treating with contaminants (gases, evaporants) surfaces which had been prepared previously under ultra high vacuum conditions.

FOOTNOTES

1. Fowler, R. H. "The Analysis of Photoelectric Sensitivity Curves for Clean Metals at Various Temperatures," Physical Review, 38(1931), 45-56.

2. Mitchell, K. Proceedings of the Royal Society (London), A146(1934), 442.

3. Mitchell, K. Proceedings of the Royal Society (London), A153(1935), 513.

4. Fan, H. Y. "Theory of Photoelectric Emission from Metals," Physical Review, 68(1945), 43-52.

5. Kane, Evan O. "Theory of Photoelectric Emission from Semiconductors," Physical Review, 127(1962), 131-141.

6. Berglund, C. N. and Spicer, W. E. "Photoemission Studies of Copper and Silver: Theory," Physical Review, 136(1964), A1030-A1044.

7. Kane, Evan O. "Simple Model for Collision Effects in Photoemission," Physical Review, 147(1966), 335-339.

8. Beckmann, Petr "Probability of Escape of Electrons Across the Surface of Photosensitive Material," Physical Review, 150(1966), 215-221.

9. Beckmann suggests (ref. 8, p. 221) the modifications which bring his treatment into agreement with that of Berglund and Spicer (ref. 7).

10. Andreev, L. Y. and Palige, Y. A. Dok. Akad. Nauk SSSR, 152(1963), 1086.

11. Dillon, J. A., Jr. and Oman, R. M. "Work-Function Measurements and Lattice Defects," Transactions, Tenth National Vacuum Symposium (Macmillan, New York, 1963), 471-474.

12. Wainfan, N., Walker, W. C. and Weissler, G. L. "Preliminary Results on Photoelectric Yields of Pt and Ta and on Photoionization of N_2 in the Vacuum Ultraviolet," J. Applied Physics, 24(1953), 1318-1321.

13. Thomas, M. T., Shimaoka, G. and Dillon, J. A., Jr. "Lattice Defects and Surface Properties of Clean Germanium," Surface Science, 6(1967), 261-278.

14. Blackmer, L. L. and Farnsworth, H. E. "Effect of the Type of Support on the Photoelectric Work Function of Silver Films," Physical Review, 77(1950), 826-829.

15. Ying, Chung Fu and Farnsworth, H. E. "Changes in Work Functions of Vacuum Distilled Gold Films," Physical Review, (February 1, 1952), 485-486.

16. Blodgett, A. J., Jr. and Spicer, W. E. "Density of States in Nickel," Physical Review Letters, 15(1965), 29-33.

17. Berglund, C. N. and Spicer, W. E. "Photoemission Studies of Copper and Silver: Experiment," Physical Review, 136(1964), A1044-A1064.

18. Blodgett, A. J. and Spicer, W. E. "Experimental Determination of the Density of States in Nickel," Physical Review, 146(1966), 390-402.

19. Kindig, N. B. and Spicer, W. E. "Band Structure of Cadmium Sulfide-Photoemission Studies," Physical Review, 138(1965), A561-A576.

20. Spicer, W. E. "Cu, Ni, Ag, and Fe Densities of States," J. Applied Physics, 37(1966), 947-952.

21. Mr. Z. Bulun prepared all samples described here and performed the x-ray analyses on each. In addition to aiding the present work, his efforts will comprise a portion of the work for his M.S. degree in Metallurgy at Syracuse University.

22. The instrument was graciously made available by the Syracuse University Metallurgy Department.

23. Jones, F. W. "The Measurement of Particle Size by the X-ray Method," Proceedings of the Royal Society (London), A166(1938),

24. Williamson, G. K. and Smallman, R. E. "Dislocation Densities in Some Annealed and Cold-Worked Metals from Measurements on the X-ray Debye-Scherrer Spectrum," Philosophical Magazine and Journal of Science, 1(1956), 34.

25. Cohen, J. B. and Hilliard, J. E. "Local Atomic Arrangements Studied by X-ray Diffraction," Metallurgical Society Conferences, New York: Gordon and Breach Science Publishers, 36(1966), 217-341.

26. Schoening, F. R. L. "Strain and Particle Size Values from X-ray Line Breadths," Acta Crystallographica, 18(1965), 975.

27. Source: McPherson Instrument Corp., Acton, Massachusetts.

28. Cary Model 31 Vibrating Reed Electrometer, Applied Physics Corp., Monrovia, California.

29. Model C 3440A, Hewlett-Packard Co., Palo Alto, California.

30. Model 562A, Hewlett Packard Co., Palo Alto, California.

31. Model CK 60-0.5M, Kepco Instr., Flushing, New York.

32. Samson, James A. R. Techniques of Vacuum Ultraviolet Spectroscopy, New York: John Wiley & Sons, 1961, p. 87.

33. Berning, P. H., Hass, G. and Madden, R. P. "Reflectance-Increasing Coatings for the Vacuum Ultraviolet and Their Applications," J. of the Optical Society of America, 50(1960), 586-597.

34. Axelrod, Norman N. "Volume Photoeffect in Metals," J. of the Optical Society of America, 56(1966), 203-209.

35. Madden, R. P. "Preparation and Measurement of Reflecting Coatings for the Vacuum Ultraviolet," Physics of Thin Films, Vol. I (G. Hass, ed.), New York: Academic Press, 1963, 123-186.

36. Veerman, Cornelis Christiaan De Afbeelding Van Plastisch Vervormde Metaaloppervlakken Door Middel Van Foto-Elektronen, Delft: Uitgeverij Waltman, 1968.

37. Donahue, T. M. "Excitation of the Lyman-α in the Night Sky," Space Science Reviews, 1(1962), 135-153. (Dissertation)

38. Donahue, T. M. and Thomas, G. "Distribution of Hydrogen in the Outer Atmosphere," Planetary and Space Science, 10(1963), 65-72.

39. Donahue, T. M. and Thomas, G. E. "Lyman α Scattering in the Earth's Hydrogen Geocorona, 2," J. of Geophysical Research, 68 (1963), 2661-2667.

40. Hinteregger, H. E., Damon, K. R. and Hall, L. A. "Analysis of Photoelectrons from Solar Extreme Ultraviolet," J. Geophysical Research, 64(1959).